

## THEORETICAL PREDICTION FOR REALIZATION OF SPECTRA-CONTROLLABLE HIGH-EFFICIENT PHOTOLUMINESCENT DEVICES BY MEANS OF SILICON NANOSTRUCTURES

F. Yonezawa, K. Nishio, J. Kōga, T. Yamaguchi<sup>a</sup>

Department of Physics, Keio University, 3-14-1 Hiyoshi, Kohoku-ku, Yokohama 223-8522, Japan

<sup>a</sup>Department of Physics, Tokyo Women's Medical University, 8-1 Kawadacho, Shinjuku-ku, Tokyo 162-8666, Japan

Electronic state calculations based on the tight-binding approximation are performed for silicon (Si) nanostructures, in order to elucidate the essential features of light-emitting Si. We take into account two types of models; the first model is Si nanostructure devoid of point-group symmetries, and the second model is amorphous Si nanostructure. By studying the band gaps and radiative recombination rates for these systems, we propose that the second model, amorphous Si nanostructure, is a good candidate for Si-based light-emitting devices.

(Received July 12, 2002; accepted July 22, 2002)

*Keywords:* Silicon nanostructures, Photoluminescent devices

### 1. Introduction

Silicon (Si) is a dominant material in the present-day microelectronics technology. However, because of its indirect band structure and band gap of 1.1 eV in the infrared region, it has not been possible to use it in light-emitting devices.

This situation might change in the near future, since in 1990, efficient, visible, and room temperature photoluminescence (PL) from porous [1] and nanocrystalline [2] Si was discovered. This discovery is remarkable from a technological point of view, because it opens the possibility to the use of Si in light emitting devices compatible with Si-based optoelectronic integrated circuits [3]. Because of its potential importance as light-emitting devices, the phenomenon has been extensively studied throughout the world, and much work has been performed on the topic. However, a detailed understanding of the exact origin and mechanism of this phenomenon has not yet been reached by now [3].

The phenomenon is also interesting from a physical point of view, since the essential mechanism has not yet been clarified for the appearance of the efficient light emission as a result of a drastic reduction of size and dimensionality of Si all the way down to the order of nanometers [3].

It is believed that the efficient luminescence in porous Si can be assigned to its nanostructures, whose band gap is blue-shifted because of the quantum confinement (QC) effect. For this reason, it is necessary to understand in detail the electronic states and optical properties of Si nanostructures in order to clarify the mechanism of the efficient luminescence. To this end, there have been a number of calculational studies on Si nanostructures, focused on the effects that the change in size bring about [4, 5, 6, 7, 8].

Previous studies have been performed on Si nanostructures with special symmetries. For example, most work on zero-dimensional systems have assumed a spherical shape with  $Td$  point-group symmetries. This assumption greatly simplifies the calculations, but is not appropriate in real physical systems. In order to elucidate the essential physics of light-emitting Si, it is necessary to study Si nanostructures with a wide variety of realistic structures.

In this work, we study Si nanostructures with various atomic configurations. Among others, we investigate two types of nanostructures; 1. Si nanostructure with no point-group symmetries [9], and 2. amorphous Si nanostructures [10, 11]. For each structural model, electronic state calculations based on the tight-binding (TB) approximation are performed, and the radiative recombination rate is calculated. From these calculations, we extract the essential aspects of realistic light-emitting Si.

## 2. Computational method

In this section, we briefly describe the calculational method we use in this work. We perform electronic state calculations based on the TB method, which allows us to treat many types of nanostructures of various sizes. Since the experimental data are in fact the average value of physical quantities from many equivalent-size nanostructures of different atomic configurations, the calculational accuracy for a particular atomic configuration is rather unimportant. The important point is to study numerous different nanostructures, and study the tendency of their behaviors as a whole. In this respect, it is best to use the TB method, which is far more efficient than first-principle electronic state calculations, and accordingly, allows us to treat a large number of different nanostructures. Since we are interested in optical properties, we need such a TB scheme as can accurately describe the conduction band of Si. In order to fulfill this requirement, we use several types of TB schemes, such as the three-center integral scheme of Ref. [12] and the  $sp^3s^*d^5$  reported in Ref. [13].

The “optical property” we calculate in this work is the radiative recombination rate, defined by the following equation [14]:

$$\frac{1}{\tau_{c,v}} = \frac{4n_0\alpha(E_c - E_v)}{m^2\hbar c^2} \left| \langle \varnothing_c | p | \varnothing_v \rangle \right|^2 \quad (1)$$

where  $n_0$  is the refractive index (we choose the value of  $n_0 = 1.2$  in this work, the experimental value of porous Si [5]),  $p$  is the momentum operator,  $\alpha$  is the fine structure constant,  $c$  and  $\hbar$  have their usual meanings, i.e., the light velocity and the Planck constant divided by  $2\pi$ , and  $E_v$  and  $E_c$  are the eigen values corresponding to valence band  $v$  and conduction band  $c$ , respectively. By expanding the wave function of band  $b$ , where  $b$  being either  $c$  or  $v$ , as  $|\varnothing_b\rangle = \sum_{i\mu} a_{i\mu}^b |i\mu\rangle$ , where  $i$  is the site index and  $\mu$  is the angular momentum, we can write the matrix element in Eq. (1) as

$$\langle \varnothing_c | p | \varnothing_v \rangle = \sum_{i\mu, j\nu} a_{i\mu}^{c*} a_{j\nu}^v \langle i\mu | p | j\nu \rangle \quad (2)$$

Since experiments are usually performed at room temperatures, we evaluate the thermal average of the radiative recombination rate by the following equation:

$$\left\langle \frac{1}{\tau} \right\rangle = \frac{\sum_n \frac{1}{\tau_{n,n'}} e^{-\frac{(E_n - E_{n'})}{k_B T}}}{\sum_n e^{-\frac{E_n - E_{n'}}{k_B T}}} \quad (3)$$

Here,  $k_B$  is the Boltzmann constant,  $T$  is the temperature,  $n$  and  $n'$  represent conduction and valence bands, respectively, and the other symbols are the same as described in the above. Equation (3) is a good approximation if the carriers are in thermal equilibrium prior to recombination, which is the case for Si nanostructures [4].

## 3. Si nanostructure without point-group symmetry

In this section, we study Si nanostructures devoid of point-group symmetries [9]. Here, one-dimensional systems, or quantum wires, are studied, in which periodic boundary condition is assigned for one direction (the [001] direction in this work) for a given unit cell.

As mentioned in the Introduction, previous studies have adopted model structures with high pointgroup symmetries. An example of such model structures is shown in Fig. 1 (a). This unit cell is the so-called  $N \times N$  wire ( $13 \times 13$  in this case), and is constructed by cutting the four equivalent  $\{110\}$  planes of bulk Si. The  $N \times N$  quantum wire has  $p\bar{4}m2$  symmetry [6]. Dangling bonds are passivated by hydrogen atoms. An  $N \times M$  unit cell can be made in an analogous fashion.

Fig. 1 (b) is an example of the model atomic configuration newly introduced in our work. These atomic configurations are constructed by randomly adding an arbitrary number of Si atoms on the surface of the structure in Fig. 1 (a). The number of Si atoms added are chosen so that it exceeds the number of initial surface bonds. Dangling bonds which inevitably appear after this procedure are passivated by hydrogen. The particular configuration shown in Fig. 1 (b) is a system with 182 Si atoms and 100 H atoms. We assume that the local crystalline configuration is preserved in all cases. In order to make the model more realistic, it is possible to energetically relax a structure such as shown in Fig. 1 (b). In separate papers (Ref. [15, 16]), we show that the effects of structural relaxation are not significant in the case studied here.

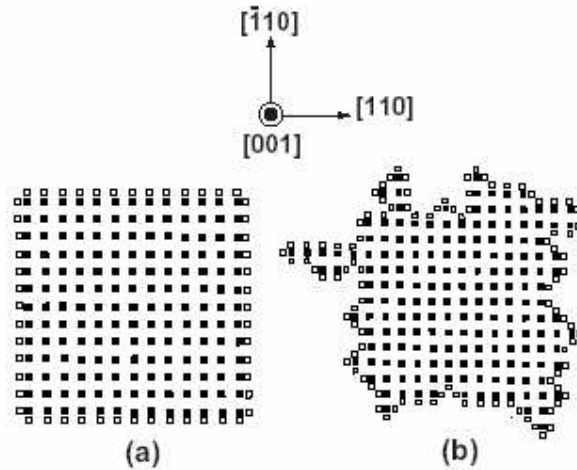


Fig. 1 Examples of the unit cell for a quantum wire model; (a) an  $N \times N$  wire and (b) a low-symmetry wire. The particular structure shown is (a)  $13 \times 13$  and (b) 182 Si atoms and 100 H atoms. The filled circles represent Si atoms, while the white circles represent H atoms. Other structures can be made in the same manner.

In Fig. 2 (a), the optical band gap is plotted against the size (linear dimension) of the model structures. The results are shown for the high-symmetry and low-symmetry wires, i.e., wires with and without pointgroup symmetry, respectively. From Fig. 2 (a), we observe that  $E_g$  shifts to the blue as the system size becomes smaller, reflecting the QC effect [4, 5, 6, 7, 8]. It is not surprising that we obtain results consistent with the QC hypothesis even for the low-symmetry systems. The interesting feature in Fig. 2 (a) is that  $E_g$  is slightly larger for the low-symmetry wires than for the high-symmetry wires in all sizes. This result implies that the blue-shift of the band gap is induced not only from the QC effect, but also from the reduction in the degree of symmetry in nanocrystals. It must be noted, however, that this difference is not substantial. From Fig. 2 (a), we conclude that the band gap of a quantum wire is mainly governed by the QC effect, with some modifications coming from symmetry properties. The physical meaning of the slight blue-shift can be understood in terms of the effective coordination number of the Si atoms. For the high-symmetry wires, the effective coordination number is high (although much lower than the bulk value of four), while for the low-symmetry wires it is lower. Therefore, when compared to the high-symmetry wires, the band width is narrower for the low-symmetry wires, which leads to a larger band gap.

We show in Fig. 2 (b) the thermally-averaged radiative recombination rate  $\frac{1}{\tau}$  (at 300 K) plotted against the PL emission energy  $E_{PL}$  for the high- and low-symmetry wires. The experimental results for porous Si, reproduced from Ref. [17], are also shown for comparison.

The relation between  $\frac{1}{\tau}$  and  $EPL$  was studied in previous works for the high-symmetry structures, and it was shown that  $\frac{1}{\tau}$  increases as  $EPL$  increases [3, 5, 4]. It was pointed out that  $\frac{1}{\tau}$  decreases rather rapidly as  $EPL$  decreases, and is inconsistent with experiments at low (<2.0 eV) energies [3, 5, 4].

We see from Fig. 2 (b) that the results for the low-symmetry unit cell wires are qualitatively as well as quantitatively different from the results of the high-symmetry wires. The results for the high-symmetry wires show that  $\frac{1}{\tau}$  is systematically lower than the experimental data. In particular,  $\frac{1}{\tau}$  decreases rapidly as  $EPL$  decreases, and is inconsistent with experiments at lower energies. On the other hand the results for the low-symmetry wires show a slower decrease in  $\frac{1}{\tau}$ , and are consistent with experiments at all energy range.

Our results show that symmetry changes the radiative recombination rate considerably for these wires, especially for low-energy transitions. The physical meaning of this consequence is explained as follows.

Firstly, in the case of bulk Si, both the conduction and valence bands have  $p$ -symmetry, which leads to zero oscillator strength. Secondly, for the high-symmetry wires, the translational symmetry of bulk Si is broken, and mixing between  $p$  and  $s$  states occur at states near or at the band edge. This leads to a finite oscillator strength. But since the symmetry of the atomic configurations and wave functions is still high, many of the terms in the summation in Eq. (2) cancel out in pairs. Finally, for the low-symmetry wires, there is no symmetry in the atomic configurations and wave functions, and all the terms in the summation in Eq. (2) effectively contribute to the oscillator strength. For this reason, the low-symmetry wires give the larger values for the oscillator strength than the high-symmetry wires.

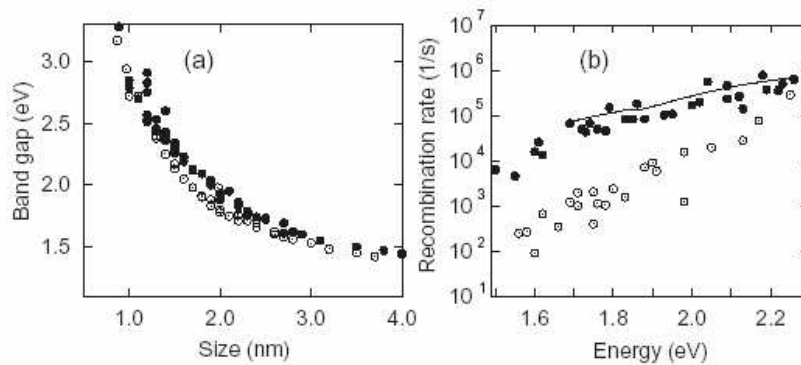


Fig. 2. (a) Band gap  $E_g$  plotted against the size of the unit cell. The open circles represent the results for the high-symmetry wires, while the filled circles represent the results for the low-symmetry wires. (b) The thermally-averaged radiative recombination time plotted against the PL emission energy  $EPL$  for the low- and high- symmetry wires. The results of PL decay measurements are shown by solid lines, reproduced from Ref. [17].

#### 4. Amorphous Si nanostructures

In the previous section, we have calculated Si nanostructures without point-group symmetries but the local crystalline structure is preserved. In this section, we deal with the case in which the local crystalline structure is *not* preserved, namely, the case of amorphous Si (a-Si) nanostructures.

We calculate a-Si quantum dots (QD) with diameters smaller than 2.4 nm. In this size region, the dominant recombination process comes from direct recombination [10, 11] instead of radiative tunneling [18, 19]. This allows us to use the same theoretical tools used in the previous section.

Our calculation procedure is as follows. We cut out 2000 ellipsoids from the CRN models generated by Barkema [20] for every set of axes ( $2a$ ,  $2b$ ,  $2c$ ), where ( $2a$ ,  $2b$ ,  $2c = 2.4$ ,  $2.0$ ,  $1.6$ , and  $1.2$  nm). We define diameter as  $D \equiv \sqrt[3]{abc}$ . We terminate the surface dangling bonds with terminators to sweep out the surface states from the band gap [10, 11]. For comparison, the QD version of the model structure of section 3 (both with and without point-group symmetry), which will hereafter be referred to simply as crystalline- (c-) Si, is also calculated.

We show in Fig.3 (a) the size dependence of the emission peak energy of a-Si QD. The definition of the emission peak energy is described in Ref [10, 11]. We also plot the experimental data for PL peak energy obtained by Park *et al.* [21]. The size sensitive PL peak energy can not be explained by the radiative tunneling scheme in which luminescence peak energy show size insensitive logarithmic behavior [19]. On the other hands, the emission peak energy of our model shows a good agreement with the peak energy of the experimental PL. The agreement of theory with experiment indicates that the dominant process of the PL is the direct recombination. The emission energy of c-Si QDs (with point-group symmetry) increases more rapidly than the peak energy of a-Si QDs as the diameter decreases. This result indicates that the quantum confinement effect has much influence on the regularly arranged structure compared with the disordered structure.

We show in Fig. 3 (b) the correlation between emission energy and recombination rate for a- and c-Si QDs without point-group symmetry [10, 11]. The recombination rate of a-Si QDs is higher than that of c-Si QDs. The recombination rate of c-Si QDs decreases rapidly as decreasing emission energy (increasing diameter), which indicates that the electronic states of c-Si QDs changes to bulk c-Si type in which dipole transition is forbidden.

The high luminescence efficiency and tunability of emission energy which covers from red- to blue-color are appealing that a-Si QD is a good candidate for the realization of Si-based light emitting devices.

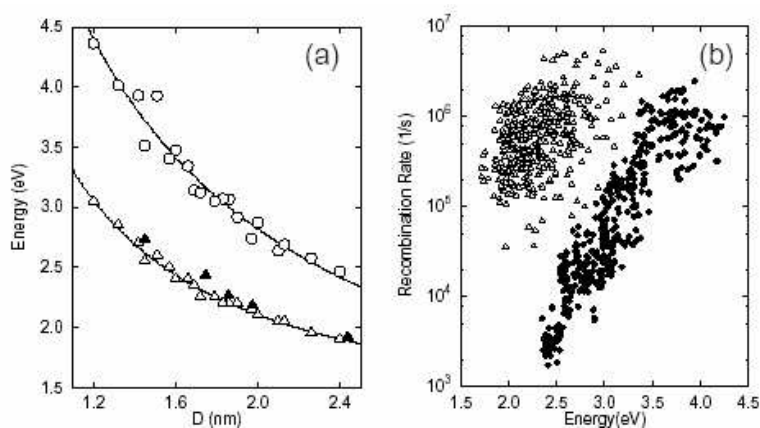


Fig. 3. (a) The size dependence of the emission peak energy of a-Si QD (open triangles) and the emission energy of c-Si QD with point-group symmetry (open circles). The experimental results of Ref. [21] are shown by filled triangles. The solid line is the least-square fit to the peak energy of a-Si QD,  $E_{em} = 1.25 + 2.37/D^{1.47}$ , and the dashed line is the least-square fit to the emission energy of c-Si QD,  $E_{em} = 0.31 + 4.87/D^{0.96}$ . (b) The correlation of the emission energy and the radiative recombination rate. The open triangles are results for a-Si QDs, and the filled circles are results for c-Si without point-group symmetry.

## 5. Conclusion

In this work, we calculated two types of non-conventional Si nanostructures, 1. model structures without point-group symmetry, and 2. amorphous Si nanostructures. We found that the radiative recombination rate is enhanced, compared to the previously-studied, high-symmetry Si nanostructures, in both cases, and that the enhancement is larger for amorphous Si nanostructures. From the results obtained, we assert that inclusion of disorder is important in studying the radiative

recombination rate of light-emitting Si, and that amorphous Si nanostructures are good candidates for realistic Si-based opto-electronic devices.

### References

- [1] L. T. Canham: *Appl. Phys. Lett.* **57**, 1046 (1990).
- [2] H. Takagi, H. Ogawa, Y. Yamazaki, A. Ishizaki and T. Nakagiri: *Appl. Phys. Lett.* **56**, 2379 (1990).
- [3] D. J. Lockwood: in *Light Emission in Silicon: From Physics to Device* (ed. D. J. Lockwood, Academic Press, 1998).
- [4] C. Delerue, G. Allan, M. Lanoo: *Phys. Rev. B* **48**, 11024 (1993).
- [5] A. J. Read, R. J. Needs, K. J. Nash, L. T. Canham, P. D. J. Calcott, A. Qteish: *Phys. Rev. Lett.* **69**, 1232 (1992).
- [6] M. S. Hybertsen, M. Needels: *Phys. Rev. B.* **48**, 4608 (1993).
- [7] J. Kōga, K. Nishio, H. Ohtani, T. Yamaguchi, F. Yonezawa: *J. Phys. Soc. Jpn.* **69**, 2188 (2000).
- [8] K. Nishio, J. Kōga, H. Ohtani, T. Yamaguchi, F. Yonezawa: *J. Non-Cryst. Solids* **293-295**, 705 (2001).
- [9] J. Kōga, K. Nishio, T. Yamaguchi, F. Yonezawa: *J. Phys. Soc. Jpn.* **70**, 3143 (2001).
- [10] K. Nishio, J. Kōga, H. Ohtani, T. Yamaguchi, F. Yonezawa: to be published in *J. Non-Cryst. Solids*.
- [11] K. Nishio, J. Kōga, H. Ohtani, T. Yamaguchi, F. Yonezawa: in preparation.
- [12] Y. M. Niquet, C. Delerue, G. Allan, M. Lanoo: *Phys. Rev. B* **62**, 5109 (2000).
- [13] J. M. Jancu, R. Scholz, F. Beltram, F. Bassani, *Phys. Rev. B.* **57**, 6493 (1998).
- [14] C. H. Henry, K. Nassau: *Phys. Rev. B* **1**, 1628 (1970).
- [15] J. Kōga, K. Nishio, T. Yamaguchi, F. Yonezawa: *J. Non-Cryst. Solids* **293-295**, 630 (2001).
- [16] J. Kōga, K. Nishio, T. Yamaguchi, F. Yonezawa: *J. Phys. Soc. Jpn.* **70**, 2478 (2001).
- [17] Y. H. Xie, W. L. Wilson, F. M. Ross, J. A. Mucha, E. A. Fitzgerald, J. M. Macaulay, T. D. Harris: *J. Appl. Phys.* **71**, 2403 (1992).
- [18] D. J. Dunstan, F. Boulitrop: *Phys. Rev. B* **30**, 5945 (1984).
- [19] R. B. Wehrspohn, J. -N. Chazalviel, F. Ozanam, I. Solomon: *Eur. Phys. J. B* **8**, 179 (1998).
- [20] G. T. Barkema, N. Mousseau: *Phys. Rev. B* **62**, 4985 (2000).
- [21] N. -M. Park, C. -J. Choi, T. -Y. Seong, S. -J. Park: *Phys. Rev. Lett* **86**, 1355 (2001).